

EVIDENCE FOR EXPANDING SUPERBUBBLES IN A GALAXY AT $z=0.7443$ ¹

NICHOLAS A. BOND, CHRISTOPHER W. CHURCHILL, JANE C. CHARLTON²

Department of Astronomy and Astrophysics
The Pennsylvania State University
University Park, PA 16802
bond, cwc, charlton@astro.psu.edu

AND

STEVEN S. VOGT
UCO/Lick Observatories
Board of Studies in Astronomy and Astrophysics
University of California, Santa Cruz, CA 96054
vogt@ucolick.org

Draft version October 27, 2018

ABSTRACT

The intervening $z = 0.7443$ Mg II absorption system in the spectrum of MC 1331 + 170 shows an unusual series of line pairs, each with $\Delta v \sim 30 \text{ km s}^{-1}$. These lines could be explained as the shells of expanding superbubbles residing in the outer regions of an edge-on spiral galaxy visible in the optical image of the MC 1331 + 170 field. The color and brightness of this galaxy make it the most likely candidate $z = 0.7443$ absorber, though two other galaxies in the quasar field could also be contributing to the Mg II absorption profile. Kinematic models of absorption from compact groups and galaxy pairs produce profiles largely inconsistent with the observed Mg II spectrum. Superbubbles would naturally generate more regular structures such as those observed. Photoionization models of the superbubble shell are consistent with the observed profile for many realistic physical conditions. In a pure superbubble model, the large velocity spread of the Mg II absorption system is inconsistent with the expected spread of a quiescent, rotating disk. This requires unusual kinematics within the host galaxy, perhaps due to a recent interaction.

Subject headings: quasars: absorption lines — interstellar medium — superbubbles

1. INTRODUCTION

Strong Mg II absorbers show complex kinematic structure consistent with a mixture of radial infall from the halo and a rotating disk (Lanzetta & Bowen 1992; Charlton & Churchill 1998; Churchill & Vogt 2001). A large variety of phenomena can contribute to the profiles, such as H I regions, H II regions, high-velocity halo clouds, and superbubbles. Strong Mg II absorbers almost always have $L_B > 0.08 L_B^*$ galaxies within 35 kpc (Steidel, Dickinson, & Persson 1994; Steidel 1995). One particular absorption system, at $z = 0.7443$, in the spectrum of MC 1331 + 170 shows multiple *pairs* of lines, each with $\Delta v \sim 30 \text{ km s}^{-1}$. There are four strong optical sources within $5''$ of the quasar, one of which is an edge-on spiral. These are the only detected optical sources which could have impact parameters less than 35 kpc.

OB associations are capable of producing large shells of swept up ISM using the energy input of stellar winds and multiple supernovae. Such structures, known as superbubbles, have been observed in nearby galaxies (Kamphuis 1993; Sungeon et al. 1999) as well as in our own galaxy (Heiles 1979; McClure-Griffiths et al. 2000). Mg II and Fe II absorption would arise within the cold superbubble shell, appearing as pairs of lines from the oppositely expanding sides of the shell intersecting the line of sight.

In our galaxy, superbubbles are detected in H I as filaments, with inferred radii ranging from 100 pc to 2 kpc (e.g. Heiles 1979). Extragalactic superbubbles are manifest as holes in the

H I map of face-on galaxies or as H I emission-line filaments in edge-on galaxies. Single structures of this type are observed with sizes similar to Galactic bubbles and masses between 10^7 and $10^8 M_\odot$. Smaller shells (even single-star stellar wind bubbles) are also thought to exist, but cannot be detected in external galaxies. Superbubbles larger than 1 kpc in radius are thought to be formed by either a merging of separate shells or by a process of self-propagating star formation (e.g. Bomans et al. 1996). The number of bubbles in a given galaxy varies dramatically from almost none to several hundred, perhaps depending on the galaxy's history of interactions.

Stellar wind bubbles for a single early-type star were first modeled by Weaver et al. (1977). Mac Low & McCray (1988) extended this concept to clusters of O and B stars, proposing Galactic superbubbles as the explanation for the H I filaments observed by Heiles (1979). According to these models, a superbubble begins as an oversized stellar wind bubble in the ISM around an OB association. The swept up material from this cavity quickly collapses into a cold, dense shell with a density greater than four times that of the ambient ISM. The shell begins expanding with the onset of the first supernovae in the OB association, which contribute their energy and metals to the superbubble. During this, the adiabatic phase, the supernovae can be approximated as a continuous energy source and the bubble radius increases as $t^{3/5}$. The interior is sparse, highly ionized, and isobaric during this phase. The continuing energy input maintains the expansion at a rate of $t^{1/2}$, in excess of the rate

¹Based in part on observations obtained at the W. M. Keck Observatory, which is operated as a scientific partnership among Caltech, the University of California, and NASA. The Observatory was made possible by the generous financial support of the W. M. Keck Foundation.

²Center for Gravitational Physics and Geometry

expected for a pure snowplow solution (Mac Low & McCray 1988).

In this paper, we explore the hypothesis that the line splittings in the $z = 0.7443$ absorber arise from expanding superbubbles in the vicinity of an observed edge-on spiral galaxy (Churchill et al. 1995). In § 2, we present the HIRES/Keck absorption profiles of detected low ionization transitions and an archival *HST*/WFPC2 image of the quasar field. In § 3, we constrain the redshifts and luminosities of the four galaxies in the quasar field using the galaxies' colors and magnitudes. We consider the possibility that galaxy pairs and compact groups give rise to the observed Mg II absorption in § 4. In § 5, we provide a description of the photoionization models used in testing the superbubble hypothesis. We discuss our results and summarize in § 6.

2. DATA AND ANALYSIS

2.1. HIRES/Keck Spectra

The spectrum of the $z = 2.084$, $V = 16.7$ quasar MC 1331 + 170 was obtained with the W. M. Keck Telescope's HIRES/Keck spectrograph (Vogt et al. 1994) on the night of 19 March 1993. The slit width was $0.861''$ (yielding $R = 45,000$). A 2×2 pixel binning (in both the cross-dispersion and dispersion directions) was used during read out. The resulting resolution is $R = 34,000$ ($v = 8.8 \text{ km s}^{-1}$ per resolution element). The wavelength coverage is 4263 to 6733 Å, with gaps above 5100 Å, because the CCD did not capture the free spectral range of the echelle orders above this wavelength. The spectrum was reduced in the usual manner using IRAF³ v2.10. All wavelengths are vacuum and heliocentric corrected.

There are four Mg II systems in the spectrum of MC 1331 + 170 at $z = 0.7443$, $z = 1.3280$, $z = 1.776$, and $z = 1.786$. Due to its unusual structure, our focus is on the $z = 0.7443$ system. The detected transitions (Fe II $\lambda 2587$, $\lambda 2600$, Mg II $\lambda \lambda 2796, 2803$, Mg I $\lambda 2853$) for the $z = 0.7443$ system are shown in Figure 1. The profile fits (solid curves) were obtained using Voigt profile decomposition. This yields the number of components, their line-of-sight velocities, column densities, and Doppler b parameters. We used MINFIT, a χ^2 minimization code of our own design (Churchill 1997). The ticks above the normalized continua in Figure 1 give component velocity centroids. Table 1 lists the resulting parameters from the Voigt profile fitting.

The equivalent width of the $z = 0.7443$ system is $W_r(2796) = 1.81 \text{ \AA}$. An *HST*/STIS spectrum that covers the C IV $\lambda \lambda 1548, 1550$ doublet is available in the archive (Program 7271). Unfortunately, the signal to noise is ~ 1 at the position of the C IV absorption, yielding no useful equivalent width limit. The other systems are also strong⁴. Damped Ly α absorption (DLA), $N(\text{H I}) \geq 2 \times 10^{20} \text{ cm}^{-2}$ is observed in the $z = 1.776$ system (Chaffee et al. 1988).

Rao and Turnshek (2000) found that 50% of Mg II absorbers with $W_r(2796) > 0.5 \text{ \AA}$ and $W_r(2600) > 0.5 \text{ \AA}$ are DLAs (also see Boissé et al. 1998). This criterion is satisfied by the $z = 0.7443$ system, but the Ly α of this system is below the Lyman limit break of the $z = 1.776$ DLA and cannot be measured. Neutral hydrogen 21-cm measurements of the $z = 0.7443$ system (Lane 2000) give $N(\text{H I}) < 1.5 \times 10^{18} \langle T_s \rangle \text{ cm}^{-2}$, where $\langle T_s \rangle$ is the spin temperature. The minimum spin temperatures

of DLAs (100 – 200 K) occur when they lie in spiral galaxies (e.g. Kanekar et al. 2000). Even if we are looking through the disk of a spiral galaxy (as we suspect), the 21-cm data do not restrict the nature of the absorber. However, the Mg II absorption arising from known DLAs has the characteristic of being totally saturated across the entire profile (Churchill et al. 2000b) and typically exhibits a total velocity spread of 50 – 100 km s^{-1} . These features are not present in this system, suggesting that it is not a DLA.

2.2. HST/PC2 Image

Images of the MC 1331 + 170 field obtained through the F702W (R) and F814W (I) filters were retrieved from the archive (Program 5351, Le Brun et al. 1997). Pipeline-reduced images for each filter were averaged and cleaned using the IRAF task GCOMBINE. The task COSMICRAYS was used to remove hot pixels. To increase the signal-to-noise ratio for presentation purposes, the R and I band images were combined. For our analysis, we use the photometry as presented in Section 2, Table 8 of Le Brun et al. 1997. Two realizations of this *HST*/WFPC2 image, with the quasar centered in the PC, are presented in Figure 2. The left-hand panel has a larger dynamic range and shows three resolved objects within $5''$ of the quasar, labeled in order of angular distance from the quasar. An additional source at $\simeq 0.8''$ is apparent upon point-spread function (PSF) subtraction of the quasar (Figure 16, of Le Brun et al. 1997). In the right-hand panel, G5 is emphasized.

3. THE MC 1331 + 170 FIELD

3.1. Procedure

The photometry of Lebrun et al. (1997) gives a limiting magnitude of 26 in R , which implies that unresolved sources at $z = 0.7443$ brighter than $\sim 0.04 L_B^*$ should be seen in the image. Because strong Mg II absorbers nearly always have $L_B > 0.08 L_B^*$ counterparts within 35 kpc (Steidel, Dickinson, & Persson 1994; Steidel 1995), we expect to detect the galaxy giving rise to the $z = 0.7443$ absorption.

There are four galaxies which could be within 35 kpc of the quasar in the *HST*/WFPC2 image (Figure 2, G2–G5, numbered as in Le Brun et al. 1997). Inspection of the sources shows an edge-on spiral morphology for G5 and an elliptical shape for G3 (also see Le Brun et al. 1997). G4 shows some structure (possibly irregular) and the location of G2 in front of the quasar makes morphology difficult to determine.

Unfortunately, redshifts for G2–G5 have not been obtained. We must, therefore, determine how likely it is that each candidate galaxy is associated with the absorber at each of the redshifts. This will allow us to assess which galaxy/galaxies could give rise to the $z = 0.7443$ absorption. We do this by comparing the apparent magnitudes and colors of each galaxy to redshifted model spectral energy distributions (SED) for different morphological types. However, we appreciate that there may not be a one-to-one correspondence between absorbers and galaxies. Two or more of the observed galaxies could give rise to absorption and lie at the same redshift (Bowen, Blades, & Pettini 1995). Additionally, DLA absorption can arise from relatively low luminosity and/or low surface brightness galaxies which are not seen in the image (e.g., Rao & Turnshek 2000; Bouché et al. 2000; also see Bowen, Tripp, & Jenkins 2000).

³IRAF is distributed by the National Optical Astronomy Observatories, which are operated by AURA, Inc., under contract to the NSF.

⁴The Mg II at $z = 1.3284$ is blended with the Fe II from the higher redshift systems (Steidel & Sargent 1992) and a precise equivalent width measurement is not possible, but we estimate $W_r(2796) = 0.8 \text{ \AA}$.

In order to obtain the L_B values expected for each galaxy at each redshift, we first obtained B and R magnitudes from model SEDs for a set of standard morphologies (Bruzual & Charlot 1993; Kinney et al. 1996). Models for E, S0, Sab, Sbc, and Scd galaxies ($\mu = 0.95, 0.30, 0.20, 0.10, 0.01$, respectively⁵) were modelled with a 16 Gyr stellar population with exponentially decreasing star formation. A redder elliptical galaxy (E2) was modeled using a composite spectrum of observed ellipticals from Kinney et al. 1996. For an irregular galaxy (Im), the observed SED of NGC 4449 was adopted (Bruzual & Charlot 1993). Two starburst models were also considered, both with a constant star formation rate, assuming a Salpeter IMF. The ages of the starburst galaxies (Starburst 1 and Starburst 2, Bruzual & Charlot 1993) are 10^6 and 10^7 years.

The K-corrections were performed by redshifting the model SEDs to the absorber redshifts and convolving them with the F702W and F814W filter response curves. A zero-point normalization was performed using the measured R band apparent magnitudes listed in Table 2 (also see Table 8 in Le Brun et al. 1997). Finally, the M_B values were calculated using $H_0 = 50 \text{ km s}^{-1} \text{ Mpc}^{-1}$ and $q_0 = 0.05$. Figure 3 shows $R - I$ color vs. redshift for the standard morphological types. The dotted lines on the figure correspond to the redshifts of the Mg II absorptions systems in the MC 1331 + 170 spectrum and the dashed lines to the colors of the four galaxies, G2–G5. Intersections of the lines represent permitted locations on the diagram of the galaxies in the field and allow us to constrain their type at each possible redshift.

3.2. Results

Table 2 summarizes the permitted morphological types and their calculated L_B (in units of L_B^* , using $M_B^* = -20.9$) at each absorber redshift (excepting $z = 1.786$ because of its proximity to $z = 1.776$).

The errors on the color of G2 and magnitude might be quite large due to the PSF subtraction of the quasar. The color of G2 makes it unlikely to be at $z = 0.7443$, and it must be an elliptical if it is at $z = 1.3284$ or $z \sim 1.8$. If only its color is considered, it could be an E or S0 at $z \sim 1.8$, but the derived M_B values give $L_B \sim 15 L_B^*$ for an E and $L_B \sim 5 L_B^*$ for an S0. Such luminous galaxies are exceedingly rare and we conclude that G2 is probably at $z = 1.3284$.

The morphology and color of G3 seem to indicate that it is an early-type galaxy, but its redshift is difficult to constrain. If at $z = 0.7443$, G3 would have $L_B \sim 0.1 L_B^*$ and could be an E, S0, or early-type spiral. Due to the low luminosity, it is uncertain whether G3 would be giving rise to strong Mg II absorption at this redshift. G3 could be an S0 at either $z = 1.3284$ with $L_B \sim 1 L_B^*$ or $z \sim 1.8$ with $L_B \sim 4.3 L_B^*$. If it is the latter, the galaxy would be unusually luminous. Therefore, it is most likely an E or S0 at $z = 0.7443$ or $z = 1.3284$.

G4 is very blue and would have to be actively star-forming to be at $z = 0.7443$. Just as with G3, however, it may not be luminous enough ($L_B \sim 0.1 L_B^*$) at this redshift to be expected to give rise to strong Mg II absorption. The irregular structure observed in the image may indicate an Im galaxy. The color and luminosity ($L_B \sim 0.1 L_B^*$) are also consistent with such a morphology at either $z = 1.3284$ or $z \sim 1.8$. The color-redshift curves converge toward $R - I \sim 0$ at high redshift for the spiral types, allowing an Scd or Sbc identification for G4 at $z \sim 1.8$.

The most striking galaxy in the MC 1331 + 170 field is G5, an edge-on spiral. This is our favored candidate for a $z = 0.7443$ absorber, with a luminosity of $L_B \sim 1 L_B^*$. The low luminosities of G3 and G4 make them marginal cases for producing such strong Mg II absorption. Additionally, the luminosity of G5 becomes larger for the higher absorber redshifts ($\sim 2 - 3 L_B^*$); thus, it ~ 10 times less likely to be at the higher redshifts. The color of G5, however, does not constrain its redshift and allows it to be a star-forming galaxy at any of the higher redshifts. If this is so, G3 or G4 would be responsible for the $z = 0.7443$ system, but their small luminosities at this redshift make this unlikely.

In conclusion, G5 is the galaxy most likely to be producing $z = 0.7443$ absorption, but G3 and G4 could also be contributing to the absorption at that redshift. If so, they would have small luminosities that make them border-line candidates for strong Mg II absorption.

4. KINEMATIC MODEL SIMULATIONS OF GROUPS AND PAIRS

Though G5 is the best candidate for the $z = 0.7443$ absorber, G3 and G4 also have colors and luminosities consistent with this redshift. Furthermore, the blue colors of G4 and G5 seem to indicate recent star formation, which could easily have been triggered by an interaction between two or more galaxies. As such, two compelling possibilities are that the line of sight passes through several members of a compact group of galaxies or through a galaxy pair, giving rise to the observed Mg II absorption profile.

Charlton and Churchill (1998) found that the kinematics of strong Mg II absorbers can be described by assuming that the absorbing clouds are located both in the disks and halos of normal galaxies. In order to synthesize an absorption line profile, we run a line of sight through a model galaxy with a given orientation, impact parameter, and size (where the size of the galaxy is defined by its luminosity). We used the luminosity and impact parameter from Table 2 as the input for each galaxy model. The orientation of galaxy G5 was set to be edge-on but, when the other galaxies were used, their orientations were chosen randomly. Each galaxy model was chosen from 75D/25H Hybrid2 in Charlton & Churchill (1998), with 75% disk clouds and 25% halo clouds, by number. In order to simulate absorption from either compact groups or galaxy pairs, the individual synthetic absorption profiles were shifted in velocity based on observed compact group or galaxy pair kinematics. We generated 1000 realizations of synthetic spectra for each.

4.1. Compact Groups

The median velocity dispersion of compact groups, 200 km s^{-1} (Hickson et al. 1992), results in profiles that have velocity spreads larger than in the $z = 0.7443$ system. A smaller velocity dispersion was required so that our models did not produce synthetic profiles with total velocity spreads inconsistent with the data. Therefore, we chose the galaxy relative velocities from HGC 22, the compact group with the minimum velocity spread (100 km s^{-1} , Hickson et al. 1992). Thus, we have already restricted ourselves to a limited region of parameter space; this is not a “typical” compact group.

Twenty-five randomly selected synthetic spectra from our three-galaxy compact group models (using G3, G4, and G5) are shown in the upper panel of Figure 5. Clearly, the velocity spreads of the clouds in the simulated spectra tend to be greater

⁵ μ is the fraction of the mass in the stars after one Gyr (Bruzual 1983)

than that in the $z = 0.7443$ system, even with the bias towards a small dispersion in galactic velocities. Also, the saturation levels in the simulated spectra tend to be higher, implying that our particular line of sight passes through less material than in an average model compact group. Finally, the regular structure of pairs in absorption, separated by $\sim 30 \text{ km s}^{-1}$, is not a characteristic feature of lines of sight through model compact groups.

4.2. Galaxy Pairs

In order to reduce the total velocity spread and saturation, we also considered models of galaxy pairs, assuming that either G3 or G4 is at $z = 0.7443$ along with G5. Again, G5 was taken to have an edge-on orientation, and the other galaxy was taken to be randomly oriented. The velocity difference between the galaxy pair is tuned to $\sim 50 \text{ km s}^{-1}$. In fact, this is a relatively typical value for field galaxy pairs.

Twenty-five randomly selected galaxy pair synthetic spectra are displayed in the bottom panel of Figure 5. Compared to the compact group synthetic profiles, a larger percentage of the pair profiles have velocity spreads and saturation levels consistent with the observed Mg II profile. However, the regular absorption line pairs we observe in the spectrum of MC 1331 + 170 are only rarely produced, even in this simple galaxy pair model.

4.3. Kinematic Model Results

The $z = 0.7443$ absorber toward MC 1331 + 170 was selected for this study because of its uniquely regular properties. As such, this is a biased study. Nonetheless, we have seen that, in 1000 Monte-Carlo simulations of galaxy pairs and in 1000 simulations of compact groups, we can only rarely produce a profile with such low levels of saturation and regular velocity splittings. However, it is difficult to quantify the shapes of the profiles in such a way that we can make direct statistical comparisons. We remind the reader that we used a compact group with an unusually small velocity dispersion. Therefore, based on this and on a visual inspection, we conclude that the observed profile is unlikely to arise from either a compact group or galaxy pair environment.

5. SUPERBUBBLE SIMULATIONS

The spectrum of the $z = 0.7443$ absorption system appears to be kinematically consistent with a line of sight intersecting the oppositely expanding sides of the “cold” shells of multiple superbubbles (Churchill et al. 1995). In order to test this hypothesis, we calculated what the column densities of Mg II and Fe II should be in the context of such a model.

5.1. The Model

The global properties of our model superbubbles are governed by the similarity solutions of Mac Low & McCray (1988) (also see Weaver et al. 1977). Models of the cold shell of the superbubbles were performed using Cloudy, version 94.00 (Ferland 1996), taking into account chemical and ionization conditions. The photoionization source consists of the ultraviolet background from quasars (Haardt & Madau 1996) and the O and B stars driving the expansion of the superbubble. The intensity of the Haardt–Madau background is set to a constant hydrogen-ionizing photon number density of $10^{-5.2} \text{ cm}^{-3}$ (as appropriate for $z \sim 1$). The stellar contribution depends on the luminosity of the parent OB association and the radius of the superbubble. Based upon our models, we find that for luminosities greater than $\sim 10^{38} \text{ ergs s}^{-1}$, the stellar spectrum

dominates at ages less than $\sim 10^7$ years. Most of the models, however, are dominated by the Haardt–Madau spectrum.

We assume the ISM to have a constant initial atomic density of $n_0 \text{ cm}^{-3}$. An OB association residing in this medium generates a total luminosity of L_{38} (in $10^{38} \text{ ergs cm}^{-3}$) through a series of supernova explosions. If each supernova produces $\sim 10^{51} \text{ ergs}$ and the OB association lasts 50 million years, the time-averaged luminosity is related to the number of supernovae by $N_{SN} \simeq 580 L_{38}$. The atomic density inside of the swept up shell is n_e (expressed in units of cm^{-3}) and the metallicity is Z , in solar units. The energy input from supernovae drives the bubble radially outward into the ISM. The similarity solution (Mac Low & McCray 1988) gives the radius of the bubble,

$$R = 0.27 (n_0/L_{38})^{-0.2} t_7^{0.6} \text{ kpc}, \quad (1)$$

where t_7 is the age in units of 10^7 years. The shell expansion speed then follows as

$$\dot{R} = 16 (n_0/L_{38})^{-0.2} t_7^{-0.4} \text{ km s}^{-1}, \quad (2)$$

which is constrained by the observed velocity splitting, Δv , of the absorption lines according to

$$\dot{R} = 0.5 \Delta v (1 - z^2/R^2)^{-1/2}, \quad (3)$$

where z is the impact parameter (to the center of the bubble) of the line of sight. This equation is not very sensitive to impact parameter unless $z/R \sim 1$. From the observed profile, $\Delta v \sim 30 \text{ km s}^{-1}$; thus, we set $\dot{R} = 15 \text{ km s}^{-1}$.

If we choose L_{38} and t_7 , we can calculate R and N_{tot} for input to the Cloudy model, where N_{tot} is the total hydrogen column density. The radius is found by combining equations (1) and (2), giving

$$R = 0.017 \dot{R} t_7 \text{ kpc}. \quad (4)$$

From equation (1), n_0 is given by

$$n_0 = L_{38} \left(16 t_7^{-0.4}/\dot{R}\right)^5 \text{ cm}^{-3}. \quad (5)$$

Finally, N_{tot} is

$$N_{tot} = 10^{21} R n_0 \text{ cm}^{-2}. \quad (6)$$

The luminosity, L_{38} (0.01,0.1,1,10), was chosen for OB associations containing between 5 and 5,000 stars (e.g. McKee & Williams 1997; Bresolin et al. 1998). The age, t_7 (0.5,1,2,4), was chosen to represent different points in the evolution of a bubble expanding for 50 million years (Mac Low & McCray 1988). The Cloudy models of the shell required that we also input $\log n_e$ (-2.5 to 2 , with intervals of 0.25). Cloudy was then run for every combination of the chosen parameters (L_{38} , t_7 , n_e , and Z). The metallicity range ($\log Z \lesssim 0$) was based upon observational constraints (see § 5.2). Each simulation was halted when the hydrogen column density (N_{tot}) calculated in Equation 6 was reached.

5.2. Simulation Results

For each L_{38} and Z , Cloudy grids were generated. In Figure 4, we show a plot of output grids from Cloudy photoionization models for the $\log Z = -1$ and $\log Z = -0.5$ cases. The thickness of the plane parallel supernova shell is plotted versus its Mg II column density. Each panel represents a different luminosity of the parent OB association (given by L_{38}). The solid lines represent the ages of the model superbubbles, corresponding (from left to right) to $t_7 = 4, 2, 1,$ and 0.5 . The dashed lines represent the hydrogen number density of the shell, which ranges from (top to bottom) $\log n_e = -3$ to $\log n_e = 2 \text{ cm}^{-3}$ in logarithmic intervals of 0.25. We picked the regions of parameter space which are in the observed Mg II column density range (see Table 1) and are consistent with observed superbubbles (Heiles 1979). These regions are enclosed by the dotted boxes.

The models produce values for n_e/n_0 over a large range, the maximum being ~ 1000 . We only plot models for which the shell is more dense than the ISM ($n_e > n_0$, where n_0 is found from Equation 5). This will probably be the case unless there is an extreme ISM density gradient (Mac Low, McCray, & Norman 1989) or we are passing through a cloudy medium (Silich et al. 1996). Real superbubbles have shell densities greater than four times the ISM densities, perhaps greater than ten times if the shells are overstable (Ryu & Vishniac 1988).

It may seem counter-intuitive that Mg II column density decreases as time increases, but the successive t_7 grid lines do not represent an evolutionary sequence. The decrease is a consequence of holding shell speed constant for all models. In order to produce the same speed at a later time, the ISM density must be lower (providing less resistance). Thus, the different t_7 lines represent varying initial conditions (see Equation 2). If you have a smaller ISM density, then you will have a smaller amount of material swept up into the shell, resulting in a smaller Mg II column density.

Increasing the luminosity of the clusters corresponds to a shift of the grid toward higher Mg II column densities and thicker shells. Increasing metallicity causes a shift in the grid towards lower Mg II column densities. We have set constraints on the value of L_{38} , so we can now constrain Z to fit observational parameter space (the dotted box). The three left-hand panels of Figure 4 show $\log Z = -1$, which is consistent with the observed Mg II column densities for $L_{38} = 0.01$ or $L_{38} = 0.1$. A grid with an increased metallicity would require a lower L_{38} (as apparent in the three right-hand panels). If $\log Z > 0$, the models require a luminosity that is too low for an OB association ($L_{38} < 0.01$). The largest OB associations contain ~ 7000 supernova progenitors (McKee & Williams 1997), corresponding to $L_{38} \sim 10$ (not shown in Figure 4). Even under these extreme conditions, we cannot place a useful lower limit on the metallicity in the shell.

We can not obtain general lower and upper limits on t_7 (though $t_7 < 5$ is a physical limit in our models, see § 5.1). The ages are limited, however, for particular combinations of L_{38} and Z . For example, the $L_{38} = 0.1, \log Z = -1$ grid in Figure 4 has only $1 < t_7 < 4$ lying within the allowed parameter space (dotted box). Presumably, the multiple bubbles giving rise to our spectrum could arise from the same burst of star formation and have similar ages and metallicities. For this to be true, a logarithmic spread of 1.5 is required in L_{38} in order to reproduce the entire range of Mg II column densities.

As with t_7 , we cannot obtain general lower and upper limits

on the shell density, n_e , but we can constrain it for particular combinations of L_{38} and Z . As can be seen in Figure 4, increasing L_{38} raises the grid and brings higher shell densities into the allowed parameter space. For example, the $L_{38} = 0.1, \log Z = -1$ grid has only $-1.5 > \log n_e > 1 \text{ cm}^{-3}$ lying within the allowed parameter space.

6. CONCLUSION AND DISCUSSION

The line pairs in the $z = 0.7443$ Mg II absorption system in the spectrum of MC 1331 + 170 are strongly suggestive of shells of expanding superbubbles. The identity of the host of the $z = 0.7443$ absorption system is not immediately obvious, but is likely to be the spiral galaxy (G5) seen in the *HST*/WFPC2 image (Figure 2). G3 and G4 are also candidates for being at $z = 0.7443$ and may form a compact group or pair with G5. However, kinematic models of galaxy pairs and compact groups seem to yield velocity spreads larger than the observed $\sim 200 \text{ km s}^{-1}$ and rarely reproduce the symmetry seen in the MC 1331 + 170 system. This evidence seems to suggest that the absorption arises in a single galaxy, either from superbubbles or random cloud distributions. Photoionization models, considering the conditions of the parent OB association and the surrounding medium, support the superbubble hypothesis without requiring fine-tuning of the specific conditions from which the superbubbles arise.

The models of superbubbles do, in fact, produce the observed Mg II column densities and velocity splittings of the $z = 0.7443$ system, but there are still some discrepancies. The $\sim 250 \text{ km s}^{-1}$ spread of our profile is the most problematic feature in the context of disk superbubbles. A typical L^* galaxy has a rotation velocity (V_0) of $\sim 220 \text{ km s}^{-1}$. If one assumes that the superbubbles follow the disk rotation, the maximum spread (V_{max}) over which they could occur is $V_{max} = V_0(1 - D/R_g)$, where D is the impact parameter and R_g is the maximum galactic radius at which superbubbles can occur. The parameter R_g is likely to be approximately equal to the optical radius of the galaxy. In M101, superbubbles are seen out to 30 kpc (Kamphuis 1993). If we assume that R_g can be as large as $\sim 40 \text{ kpc}$, we get only $V_{max} \sim 100 \text{ km s}^{-1}$. For G5 at $z = 0.7443$, the impact parameter is $20 \text{ h}^{-1} \text{ kpc}$.

There are several possible explanations for the large spread in the $z = 0.7443$ Mg II absorber: 1) A merger is inducing globular cluster formation in the halo (Ashman & Zepf 1992; Zepf & Ashman 1993) and the clusters are creating superbubbles. 2) Superbubbles are forming within tidal debris from a recent interaction (Kniermann et al. 2000; Gallagher 2001). A line of sight through tidal debris can create velocity spreads as large as 1000 km s^{-1} (Gallagher 2001). 3) Some of the superbubbles are outliers in velocity space, possibly located within a companion dwarf galaxy (Mac Low & Ferrara 1999). 4) Some of the absorption lines are not from superbubbles and lie outside of the disk. This absorption could arise in halo clouds or in dwarf galaxies.

Womble, Junkkarinen, and Burbidge (1991) point out that large velocity spreads in edge-on galaxies are better explained by chimneys, worms, or superbubbles blowing out into the halo. These are processes known to occur at the end of a superbubble's lifetime when the shell accelerates through a density gradient into the halo. The shell then fragments due to Rayleigh-Taylor instabilities and the bubble begins expelling material out of the disk. This process is quite messy, however, and is not likely to give rise to such evenly split lines.

Our spectrum shows no more than six superbubbles within the line of sight, each ~ 10 pc thick (Mac Low, McCray, & Norman 1989); thus, there must be a substantial path length through the ISM in between the superbubbles. Why don't we see dominating absorption from the ISM between the superbubbles? The simplest explanation is that the filling factor of the superbubbles is so large that the path length through the ISM makes a negligible contribution to the absorption. Observations of HI holes in nearby galaxies (Kamphuis 1993) give maximum covering factors of ~ 0.3 ; however, they are only sensitive down to $R \sim 0.5$ kpc. Another possible explanation is that OB associations reside in regions of enhanced density and the superbubbles sweep the densest material into their shell before reaching the sparse, intervening material. Finally, the parent OB associations themselves are at unusual velocities

with respect to most of the ISM material. This separation in velocity space may arise if the bubbles are localized in a certain part of the disk or exist in a star-forming tidal tail nearby. The lines at ~ -100 km s $^{-1}$ in Figure 1 show less symmetry than the others and could be arising from ISM clouds in the disk.

We acknowledge support from the NSF/REU program and NASA/LTSA through grant NAG5-6399. We would like to thank Mordecai-Mark Mac Low for his insightful comments. We thank Janet Geoffroy for the use of her spectral integration code which we used to calculate galaxy colors. We also benefit from useful conversations with Matt Bershady, Niel Brandt, Robin Ciardullo, Jenn Donley, Rajib Ganguly, Dick McCray, Jane Rigby, Ken Sembach, and Steinn Sigurdsson.

REFERENCES

- Ashman, K. M. & Zepf, S. E. 1992, *ApJ*, 384, 50
 Boissé, P., Le Brun, V., Bergeron, J., & Deharveng, J.-M. 1998, *A&A*, 333, 841
 Bomans, D. J., de Boer, K. S., Koornneef, J., & Grebel, E. K. 1995, *A&A*, 313, 101
 Bouché, N., Lowenthal, J. D., Charlton, J. C., Bershady, M. A., Churchill, C. W., & Steidel, C. C. 2000, *ApJ*, submitted
 Bowen, D. V., Blades, J. C., & Pettini, M. 1995, *ApJ*, 448, 634
 Bowen, D. V., Tripp, T. M., & Jenkins, E. B. 2000, *AJ*, submitted (astro-ph/0011134)
 Bresonlin, F., Kennicutt, R. C., Ferrarese, L., Gibson, B. K., Graham, J. A., Macri, L. M., Phelps, R. L., Rawson, D. M., Sakai, S., Silbermann, N. A., Stetson, P. B., & Turner, A. M. 1998, *AJ*, 116, 119
 Bruzual, A. G., & Charlot, S. 1993, *ApJ*, 405, 538
 Charlton, J. C., & Churchill, C. W. 1998, *ApJ*, 499, 181
 Chaffee, F. H., Black, J. H., & Foltz, C. B. 1988, *ApJ*, 335, 584
 Churchill, C. W., Vogt, S. S., Steidel, C. C., 1995, From metal-line absorption profiles to halo kinematics. In: Meylan G. (ed.) *QSO absorption lines*, Springer, Berlin, p.153
 Churchill, C. W. 1997, Ph.D. Thesis, University of California, Santa Cruz
 Churchill, C. W., Mellon, R. R., Charlton, J. C., Jannuzi, B. T., Kirhakos, S., Steidel, C. C., & Schneider, D. P. 2000a, *ApJS*, 130, 91
 Churchill, C. W., Mellon, R. R., Charlton, J. C., Jannuzi, B. T., Kirhakos, S., Steidel, C. C., & Schneider, D. P. 2000b, *ApJ*, 543, 577
 Churchill, C. W. & Vogt, S. S. 2001, *ApJ*, submitted
 Ferland, G. 1996, Hazy, University of Kentucky, Internal Report
 Gallagher, S. C., Charlton, C. C., Hunsberger, S. D., & Zaritsky, D. 2001, submitted
 Haardt, F. & Madau, P. 1996, *ApJ*, 461, 20
 Heiles, C. 1979, *ApJ*, 229, 533
 Hickson, P., de Oliveira, C. M., Huchra, J. P., & Palumbo, G. G. C. 1992, *ApJ*, 399, 353
 Kamphuis, J. 1993, Ph.D. Thesis, University of Groningen
 Kanekar, N., Chengalur, J. N., Subrahmanyan, R., & Petitjean, P. 2000, *A&A*, in press (astro-ph/0012079)
 Kniermann, K. A., Hunsberger, S. D., Gallagher, S. C., et. al., 2000, *ApJ*, submitted
 Kinney, A. L., Calzetti, D., Bohlin, R. C., McQuade, K., Storchi-Bergmann, T., & Schmitt, H. R. 1996, *ApJ*, 467, 38
 Lane, W. M. 2000, Ph.D. Thesis, Rijksuniversiteit Groningen
 Lanzetta, K. M. & Bowen, D. V. 1992, *ApJ*, 391, 48
 Le Brun, V., Bergeron, J., Boissé, P., & Deharveng, J. M. 1997, *A&A*, 321, 733
 Mac Low, M.-M., & McCray, R. 1988, *ApJ*, 324, 776
 Mac Low, M.-M., McCray, R., & Norman, M. L. 1989, *ApJ*, 337, 141
 Mac Low, M.-M. & Ferrara, A. 1999, *ApJ*, 513, 142
 McClure-Griffiths, N. M., Dickey, J. M., Gaensler, B. M., Green, A. J., Haynes, R. F., & Wieringa, M. H. 2000, *AJ*, 119, 2828
 McKee, C. F. & Williams, J. P. 1997, *ApJ*, 476, 144
 Rao, S. M. & Turnshek, D. A. 2000, *ApJS*, in press
 Ryu, D., & Vishniac, E. T. 1988, *ApJ*, 331, 350
 Šilich, S. A., Franco, J., Palouš, J., & Tenorio-Tagle, G. 1996, *ApJ*, 468, 722
 Steidel, C. C. & Sargent, W. L. W. 1992, *ApJS*, 80, 1
 Steidel, C. C., Dickinson, M. & Persson, E. 1994, *ApJ*, 437, L75
 Steidel, C. C. 1995, in *QSO Absorption Lines*, ed. G. Meylan (Garching: Springer-Verlag), 139
 Sungeon, K., Dopita, M. A., Staveley-Smith, L., & Bessell, M. S. 1999, *AJ*, 118, 2797
 Vogt, S. S., et al. 1994, in *Proc. SPIE Conf. 2198, Instrumentation in Astronomy VII*, edited by D. L. Crawford and E. R. Craine (SPIE, Bellingham, WA), p. 362
 Weaver, R., McCray, R., Castor, J., Shapiro, P., & Moore, R. 1977, *ApJ*, 218, 377
 Whitmore, B., Zhang, Q., Leitherer, C., Fall, S. M., Schweizer, F., & Miller, B. 1999, *AJ*, 118, 1551
 Womble, D. S., Junkkarinen, V. T., & Burbidge, E. M. 1991, *ApJ*, 388, 55
 Zepf, S. E. & Ashman, K. M. 1993, *MNRAS*, 264, 611

TABLE 1
CLOUD PROPERTIES FOR Q1331+170

Cloud $\langle v \rangle$ [km s ⁻¹]	Mg II		Fe II		Mg I	
	log N [cm ⁻²]	b [km s ⁻¹]	log N [cm ⁻²]	b [km s ⁻¹]	log N [cm ⁻²]	b [km s ⁻¹]
-140.7	11.81 ± 0.08	5.01 ± 1.68	< 11.89	...	< 10.80	...
-117.9	13.15 ± 0.01	9.09 ± 0.16	12.82 ± 0.03	8.33 ± 0.93	< 10.78	...
-90.2	13.05 ± 0.01	4.70 ± 0.12	12.61 ± 0.04	4.81 ± 0.85	11.02 ± 1.15	~ 9.5
-71.4	12.63 ± 0.01	7.13 ± 0.37	12.07 ± 0.19	2.19 ± 1.57	< 10.80	...
-47.9	12.62 ± 0.08	6.29 ± 0.59	11.62 ± 0.06	0.31 ± 0.08	< 10.84	...
-32.8	13.22 ± 0.02	13.22 ± 0.68	12.87 ± 0.04	13.54 ± 1.79	11.21 ± 0.22	4.03 ± 2.87
-6.9	13.26 ± 0.02	4.03 ± 0.20	13.25 ± 0.04	3.57 ± 0.26	11.81 ± 0.04	5.50 ± 0.80
2.1	13.03 ± 0.04	10.33 ± 0.58	12.54 ± 0.09	3.87 ± 1.09	< 10.75	...
37.6	12.01 ± 0.06	5.88 ± 1.19	< 11.82	...	< 10.80	...
63.0	12.21 ± 0.04	8.65 ± 1.10	12.52 ± 0.22	39.46 ± 22.98	< 10.80	...
103.4	13.08 ± 0.02	13.33 ± 0.56	12.83 ± 0.06	12.21 ± 1.71	11.21 ± 0.28	12.81 ± 8.38
121.4	13.08 ± 0.02	7.77 ± 0.23	12.45 ± 0.08	6.15 ± 1.24	11.09 ± 0.30	~ 2.6
148.3	13.47 ± 0.01	9.07 ± 0.12	13.31 ± 0.01	9.75 ± 0.38	11.43 ± 0.07	7.59 ± 1.58

TABLE 2
Q1331+170 FIELD ANALYSIS SCENARIOS

Galaxy	D [']	R	I	0.7443			1.3284			1.776		
				D [kpc]	Type	Luminosity [L*]	D [kpc]	Type	Luminosity [L*]	D [kpc]	Type	Luminosity [L*]
2	0.75	24.9	23.8	3.61	4.36	<i>E</i>	3.57	4.63	<i>E</i>	14.5
3	1.58	25.1	24.4	7.61	<i>S0</i>	0.08	9.18	<i>S0</i>	1.09	9.76	<i>S0</i>	5.14
4	2.86	24.2	24.2	13.77	<i>E</i>	0.08	16.62	<i>S0</i>	0.163	17.67	<i>S0</i>	4.28
5	3.86	21.40	21.47	18.58	<i>SB</i>	0.12	22.43	<i>SB</i>	0.498	23.84	<i>SB</i>	0.208
					<i>Im</i>	1.16		<i>Im</i>	2.12		<i>Im</i>	0.822
					<i>SB</i>			<i>SB</i>			<i>SB</i>	2.71

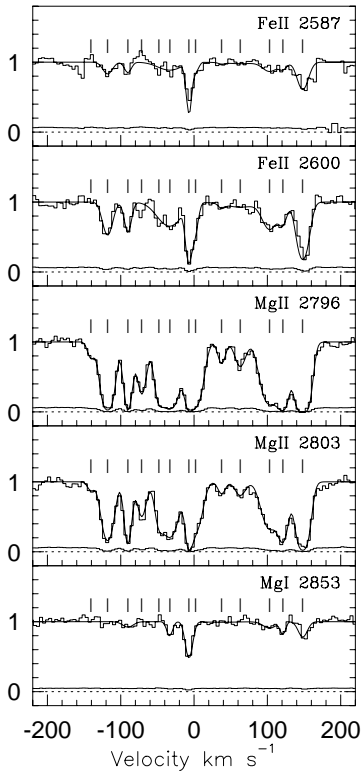


FIG. 1.— The HIRES/Keck spectrum of the $z=0.7443$ system toward Q1331+170 showing transitions detected at $> 5\sigma$ aligned in rest frame velocity space. The solid lines represent a model from a simultaneous Voigt profile fit to the spectra, with the ticks marking individual components.

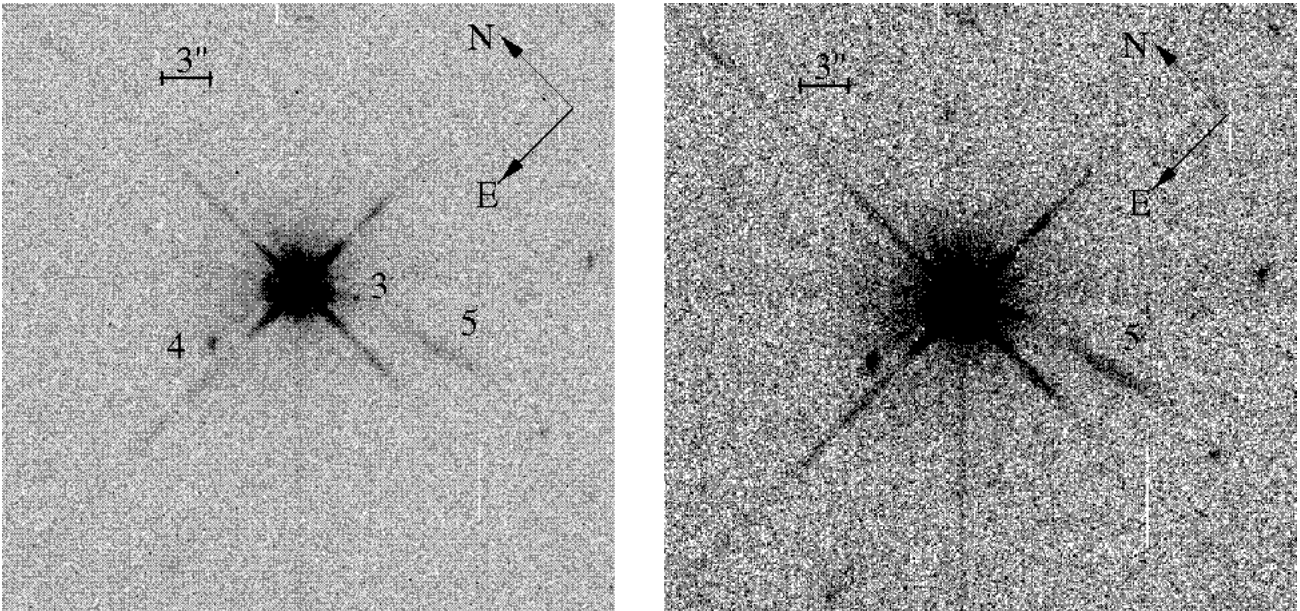


FIG. 2.— Two images, each with a different dynamic range, of the MC 1331 + 170 field combining the R (F702W) and I (F814W) filters. Galaxies are numbered G3 through G5, in order of distance from the quasar (at center). G2 is not labeled because of its proximity to the quasar and can only be resolved via PSF subtraction. The left-hand panel emphasizes G3 and G4 and the right-hand panel emphasizes G5 (for presentation purposes only).

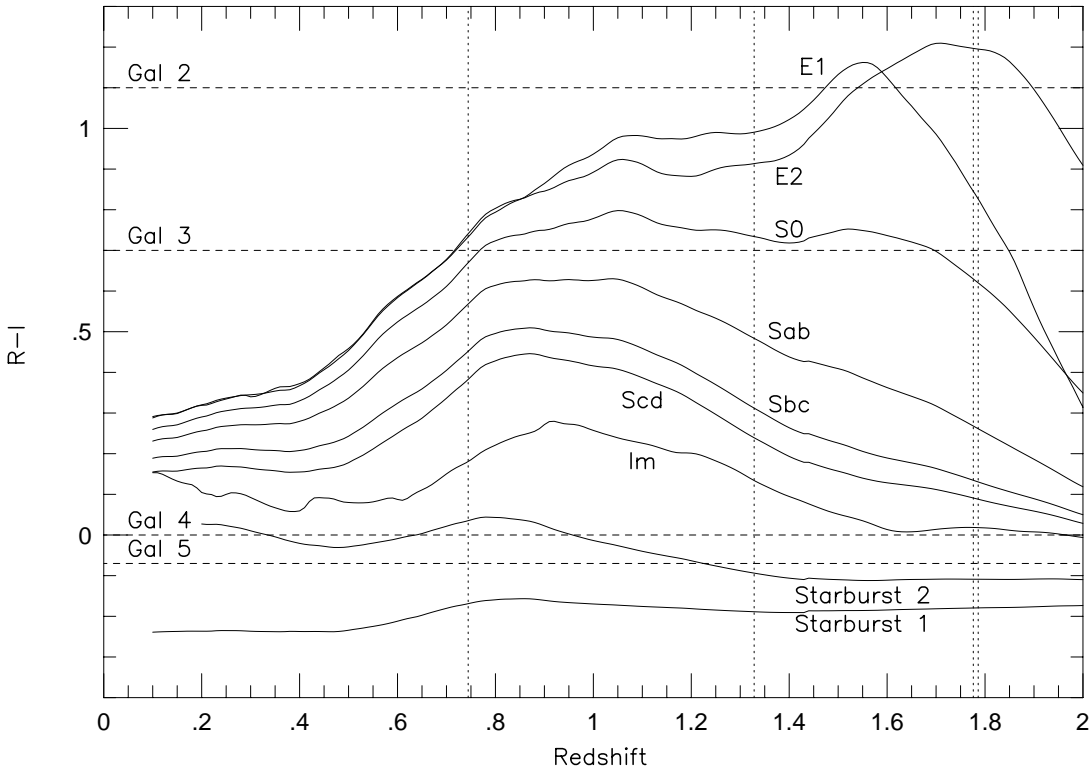


FIG. 3.— A color-redshift diagram plotted of model spectral energy distributions representing a variety of morphological types (Bruzual & Charlot 1993; Kinney et al. 1996). The dotted vertical lines denote the redshifts of the absorption systems in the spectrum of Q1331+170 and the dashed horizontal lines denote the colors of the sources in the optical field.

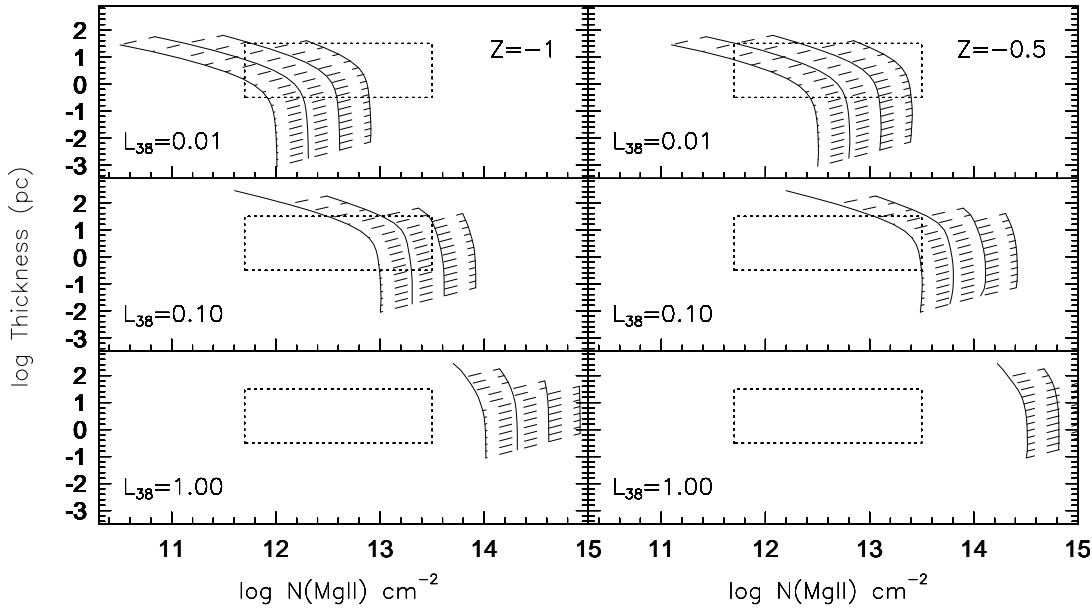


FIG. 4.— Output grids from Cloudy photoionization models for the $\log Z = -1$ and $\log Z = -0.5$ cases. Each plot of shell thickness vs. Mg II column density in a column presents a box that represents a different luminosity input from the parent OB association (given by L_{38}). From left to right, the solid curves represent the ages of the model superbubbles, corresponding to $t_7 = 4, 2, 1,$ and 0.5 . The dashed curves represent hydrogen number densities in the shell which are (from top to bottom) $\log n_e = -3$ to 2 cm^{-3} in logarithmic intervals of 0.25 . The boxes in the center of the plots represent expected parameter ranges based on observed superbubbles.

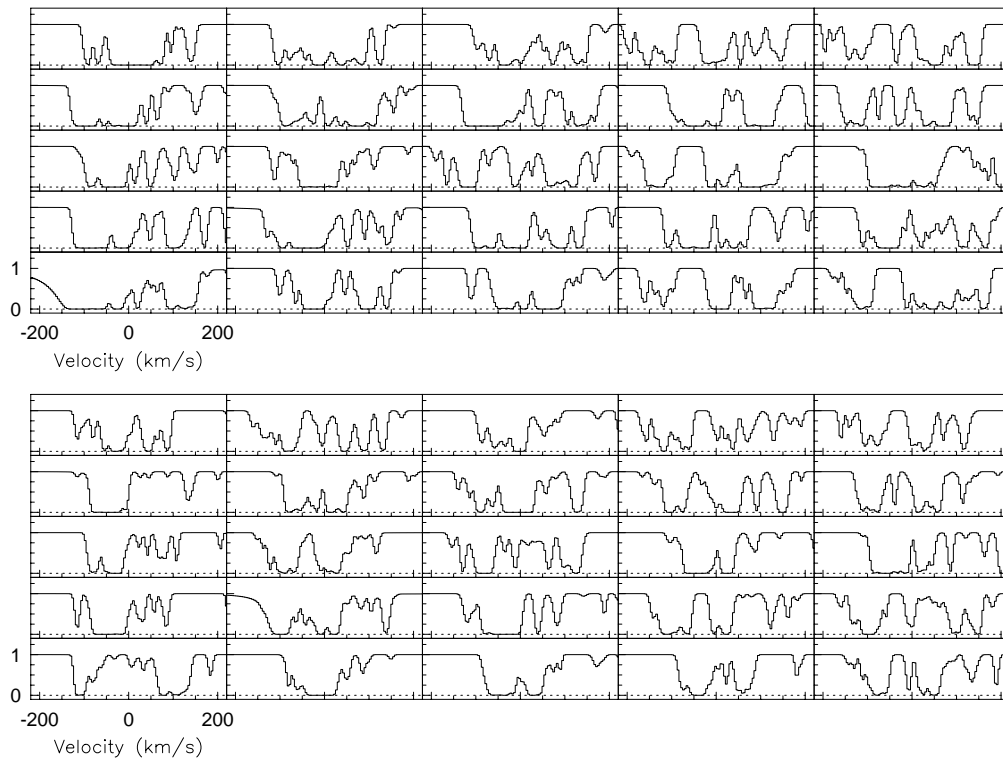


FIG. 5.— Spectra generated from 25 models of three-member compact groups (top panel) and 25 models of galaxy pairs (bottom panel).